

Wind spectral characteristics on fatigue responses of towerbase and moorings of a floating offshore wind turbine

Ikpoto E. Udoh* and Jun Zou

*Houston Offshore Engineering / Atkins, a member of the SNC-Lavalin Group,
17220 Katy Freeway, Suite 200, Houston, TX 77094, USA*

(Received December 7, 2018, Revised March 20, 2019, Accepted March 25, 2019)

Abstract. The tower-platform interface and mooring system of floating offshore wind turbines (FOWTs) are some of the most critical components with significant influences on overall project costs. In addition to satisfying strength requirements, it is typical and vital to meet fatigue criteria for a service life of 25 years or more. Wind spectra characteristics considered in analysis can penalize fatigue designs, leading to unnecessary costs. The International Electrotechnical Commission (IEC, 2009) recommends the use of site-specific wind data (spectrum, turbulence intensity, etc.) in design of FOWTs, but for offshore sites it is often the case that such data is unavailable and land-based data are used as surrogates in design. For such scenarios, it is worth investigating whether such alternative approach is suitable and accurate, and understanding the consequence of the selection of wind spectral characteristics on fatigue design. This paper addresses the impact of the subsequent selection on fatigue responses of towerbase and mooring system in a FOWT, as a sequel to the paper by Udoh and Zou (2018) which focused on impacts on strength design. The 5 MW semi-submersible FOWT platform with six mooring lines implemented in the preceding study is applied in analysis. Results indicate significant variations in resulting fatigue life with considered wind parameters. Thus, it is critical to apply proper wind spectra characteristics for analysis and design of FOWTs to avoid unnecessary conservatism and costs. Based on the findings of this study, more explicit guidance on the application of turbulence intensities for IEC-recommended models in offshore sites could lead to more accurate load estimates in design of FOWTs.

Keywords: towerbase; mooring line; fatigue; floating; wind turbine; spectra

1. Introduction

Interest in offshore wind power is growing at a rapid pace worldwide. A common theme among established offshore wind markets (Europe, United Kingdom and Asia) and growing markets like the United States, is the focus on cost reduction and improved efficiency. Incentives currently being provided by government agencies to enhance the viability of offshore wind developments may not be sustainable long term. Developers and investors are eager to establish concepts, methods, procedures, etc. across the value chain, that will guarantee low-cost delivery of offshore wind technology and services. A close assessment of engineering characteristics of FOWTs is a necessary aspect of the overall effort towards cost minimization in wind energy developments.

*Corresponding author, Ph.D., E-mail: ikpoto.udoh@atkinsglobal.com

Effective cost control in FOWT projects can only be achieved if the major drivers of significant costs are understood. The mooring system and tower-platform interface (hereafter referred to as the towerbase) connections in FOWTs can account for a significant percentage of the overall project cost, and an understanding of the elements that influence their design, and ultimately the associated costs, is critical for attaining cost-effective designs. Although adequate designs of these two components must satisfy strength and fatigue requirements, this paper focuses on the latter. The hypothesis made here is that fatigue performance of the tower-platform connection and mooring lines are sensitive to the choice of wind spectrum and spectral parameters. Characteristics (e.g. turbulence intensity) of IEC-recommended land-based wind spectra differ in trends and magnitude from offshore-based spectra. In this study, the Kaimal wind spectrum is used as the representative land-based spectrum, with turbulence intensities recommended by IEC (2005) for onshore sites. The Froya spectrum is used as the representative model for offshore sites. It is understood that the Froya model has been recommended by DNV for situations where low-frequency wind energy is important (DNV, 2007), and by API Bulletin 2INT-MET for the modeling of tropical cyclone winds (ABS, 2015). On the latter, wind speed data used in Anderson and Lovseth (2006) in the development of the Froya model range from 10 to 27 m/s; here the authors compared three different turbulence intensity models including a linear model and concluded that each of them provided good approximation to the experimental data, and showed that extrapolating the linear turbulence intensity model for wind speeds higher than 27 m/s would lead to slightly higher (more conservative) designs. Based on the recommended linear turbulence intensity model in Anderson and Lovseth (2006), this study assumes that the Froya model can be extrapolated on the low wind speed end of the data (i.e., below 10 m/s) and implements the spectrum for the full range of operational wind speeds of the turbine (4 to 25 m/s). Wave loads, and wave-induced fatigue are intentionally excluded in this study, as the focus is on the impact of wind loads on the towerbase and mooring system.

Development of the Kaimal model dates to the 70s (Kaimal *et al.* 1972, 1976); these studies led to the Kaimal spectrum with coherence, which considers the behavior of spectra and cospectra of turbulence in the surface layer using wind velocity and temperature. The experimental site used in acquiring data for the studies conducted by Kaimal *et al.* (1972, 1976) was a flat onshore site, from which data was obtained at specified elevations. To the contrary, the Froya turbulence wind model is derived based on wind turbulence data obtained at exposed sites along the western coast of Norway (Anderson and Lovseth, 2006, 1992).

Regarding mooring system analysis in FOWTs, some researchers have addressed improvement of analysis methods and integration of mooring analysis tools with aero-hydro programs (Masciola *et al.* 2011), and the influence of mooring line dynamics on a FOWTs (Masciola *et al.* 2013). Other recent studies (Udoh and Zou 2016, Udoh *et al.* 2016, Udoh and Zou 2018) have studied the effect of wind turbulence on towerbase reactions and mooring line tensions in FOWTs and have shown these effects to be significant under certain conditions. Homb (2013) investigated the fatigue of mooring lines in the Hywind Demo FOWT, but his work considered a combination of wind and wave loadings and the results are interpreted in that context. Although these previous studies have been insightful regarding the current subject, the impact of spectral characteristics on the wind-induced fatigue behavior or potential of the towerbase and mooring lines has not been explicitly addressed. Therefore, it is our goal in this study to show the impact of wind spectral characteristics on the fatigue response of towerbase and mooring lines and illustrate the importance of properly modeling wind fields in estimation of fatigue life for mooring lines.

Table 1 Natural / Eigen Periods of Platform, Tower and Blades

Platform Mode	Natural	Tower Mode	Eigen	Blade Mode	Eigen
	Period		Period		Period
	[sec]		[sec]		[sec]
Surge	69.5	Fore-Aft mode 1	2.23	Flapwise mode 1	1.48
Sway	68.0	Side-to-Side mode 1	2.27	Edgewise mode 1	0.90
Heave	20.0	Fore-Aft mode 2	0.37	Flapwise mode 2	0.52
Roll	24.5	Side-to-Side mode 2	0.46	Edgewise mode 2	0.25
Pitch	24.5	Twist mode 1	0.56		

2. System properties and wind spectra models

2.1 System properties

As this study is a sequel to Udoh and Zou (2018), the Paired-Column Semi-Submersible Floating Wind Foundation (P-C FWF) is the floater implemented in analysis, and the characteristics of the platform and turbine are discussed in Udoh and Zou (2018) – these details were excluded from this sequel for brevity. Table 1 shows the natural periods of the platform, and modal periods of the tower and blades. To avoid resonance responses at the blade rotational and passing frequencies, the tower flexural properties are optimized such that its eigen periods are away from the blade natural periods. The actual height of the tower is 72.6 m, and its distributed mass and flexural properties are given in the Appendix. A point mass of 350,000 kg, corresponding to the tovertop mass of the NREL turbine, is used in calculating the tower eigen periods. Eigen modes of the blade are based on the distributed blade properties of the NREL 5 MW turbine (Jonkman *et al.* 2009).

2.2 Wind spectra and modeling considerations

Mathematical representations of Kaimal and Froya wind spectra used in analysis are presented in Udoh and Zou (2018). Wind field grid resolutions used in analysis are reported in Table 2. Since wind-induced fatigue depends to some extent on the spectral distribution of wind energy, it is imperative to understand whether the energy distributions vary with wind field resolution. For each spectrum type, one relatively high and one relatively low resolution of the wind field is considered. In Turbsim (Section 3.4), the Froya spectrum (being a non-IEC model) has a limitation on the upper limit of wind field resolution, whereas the Kaimal model does not; this limitation can vary with wind speed, among other internal model parameters. The higher grid resolution used for the Froya model (15.8 m x 7.6 m), is the lower of the two wind field resolutions modeled with the Kaimal spectrum. Turbulence intensities used in wind modeling are shown in Fig. 1. It is noteworthy that the IEC Class C turbulence intensity is in reversed trend compared to Froya

spectrum for low mean wind speeds (1.5 to ~10 m/s); one of the main goals of this paper is to assess the impact of this distinction in turbulence intensities on fatigue responses of mooring lines and the towerbase. An important point to make in Fig. 1 is that at 10 m/s (which is the lower bound of experimental data used in Anderson and Lovseth for the Froya spectrum), the IEC Class C turbulence intensity is about 2.3 times the Froya turbulence intensity. It is therefore possible, that even without extrapolating the Froya spectrum below 10 m/s, significant differences may ensue in fatigue responses between the two spectra types considered. The extent to which such difference in turbulence intensity amounts to notable differences in actual fatigue life can be influenced significantly by the probability of occurrence of the wind speed. While we acknowledge that it is typical to have varying probabilities of occurrence for different wind speeds, in this study the probability of occurrence is assumed to be equal for all wind speed groups to enhance the delineation of the pure wind spectra-induced effects.

Table 2 Wind Field Grid Resolutions

Spectrum Type and Grid Resolution		Grid name Alias	Grid Spacing in Z [m]	Grid Spacing in Y [m]
Froya	Froya Low Resolution	Froya-L	16	30
	Froya High Resolution	Froya	7.6	15.8
Kaimal	Kaimal Low Resolution	Kaimal	7.6	15.8
	Kaimal High Resolution	Kaimal-H	7.6	9.6

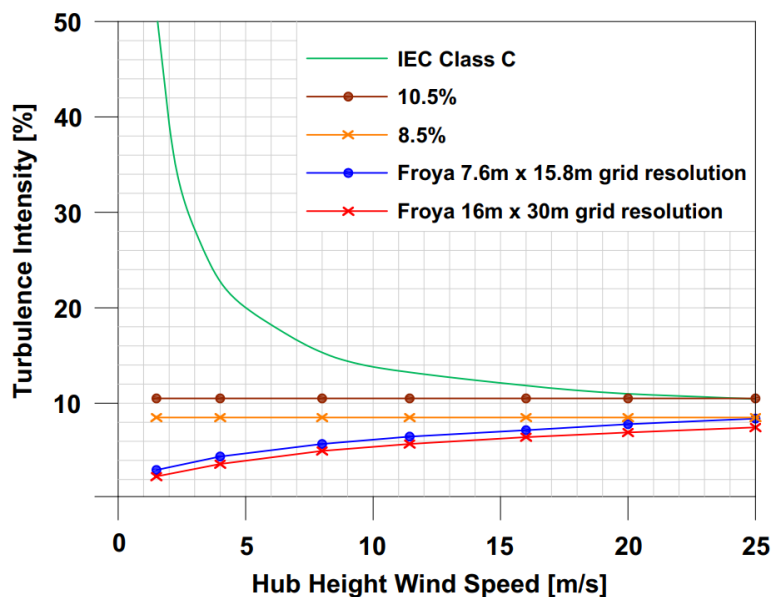


Fig. 1 Turbulence Intensity Curves Applied in Analysis

2.3 Mooring system properties

There are six mooring lines in the system; plan and elevation views of the mooring system are presented in Figs. 2 and 3, respectively. Chain properties are given in Table 3.

Table 3 Properties of Studless Mooring Chain

Parameter	Unit	Values
Grade	-	R3
Diameter ¹ /Dimension	[mm]	127
Weight in Water ³	[kg/m]	281.0
MBL3	[kN]	10888
Pre-Tension at hang-off location	[kN]	817.5
Vertical Load	[kN]	600 per line
Pay-out Angle relative to vertical	[deg]	42.8

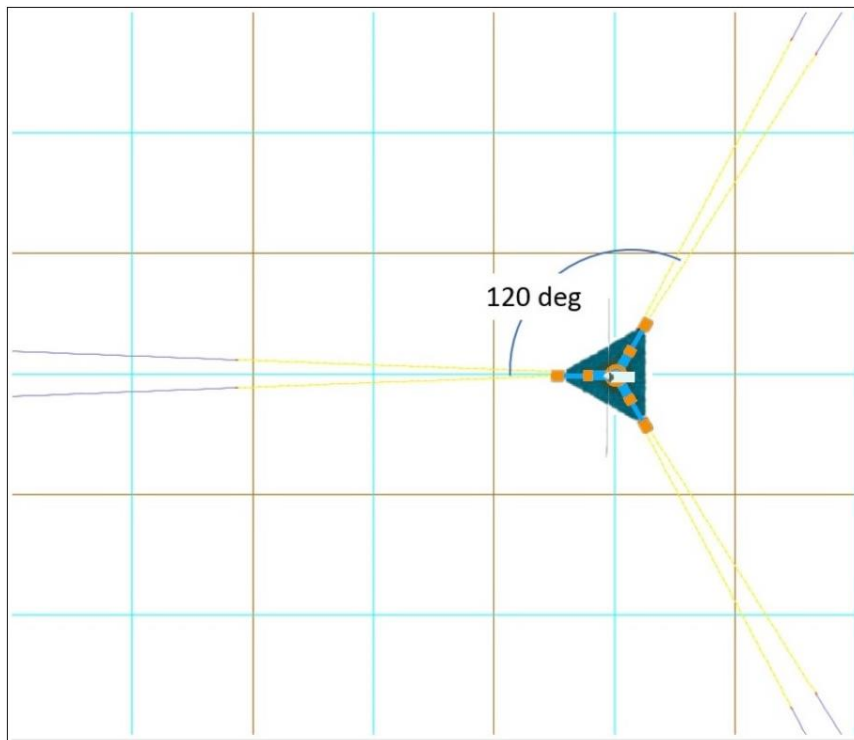


Fig. 2 Plan View of Mooring System Layout

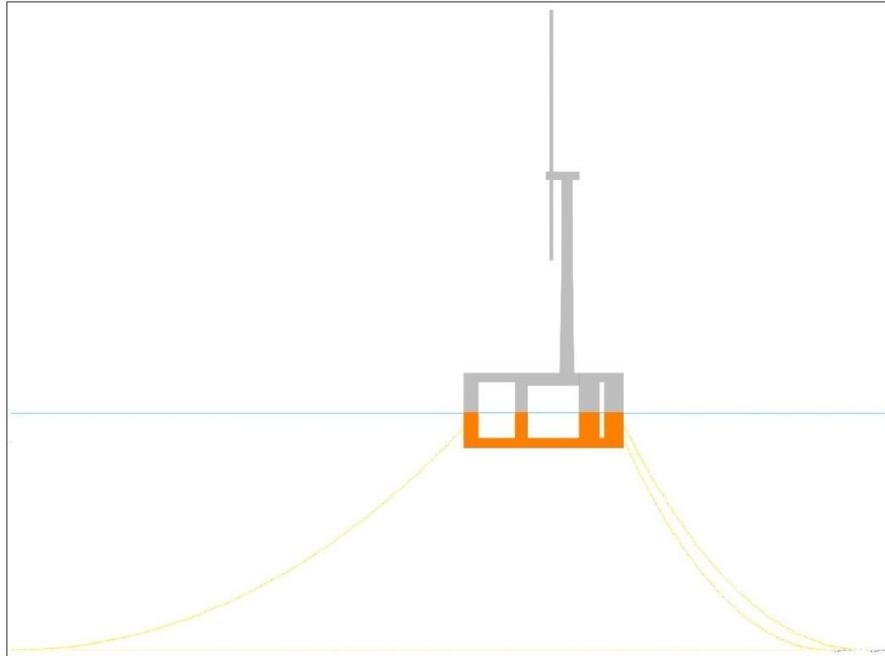


Fig. 3 Elevation View of Mooring System Layout

3. Analysis

3.1 Analysis methodology

Coupled analysis is carried out in time domain using FAST (Jonkman and Buhl 2005) and OrcaFlex (Orcina Ltd.) as the two main programs. Wind coefficients (Fig. 4) derived from correlated WINDOS (Maritime Research Institute, 2007) models are implemented in analysis. In each time-step of analysis, FAST combines the hydrodynamic loads received from OrcaFlex with aerodynamic loads calculated in FAST, to determine the instantaneous global motions, and dynamics of the tower, nacelle, blades and turbine components. Once that is completed, FAST transfers the resulting platform positions and velocities from the previous time-step to OrcaFlex for the next calculation of platform loads, and the process is repeated until the target simulation time is reached – this interactive analysis process is enabled by a dynamic link library called FASTLink (Orcina, Masciola *et al.* 2011). BMODES (Bir 2007) is used in estimating the tower eigen modes for analysis. Turbsim (Jonkman and Kilcher 2012) is applied in generating full-field turbulent winds. The program has been widely implemented with common spectral models such as Kaimal and Froya (known in Turbsim as API) models.

WAMIT (WAMIT Inc., 2006) is used in generating hydrodynamic added mass and radiation damping, while mooring line dynamics are derived from OrcaFlex. Viscous damping applied in coupled analysis are derived from model test correlation analysis for similar floating structures and are applied consistently for all wind spectra in analysis.

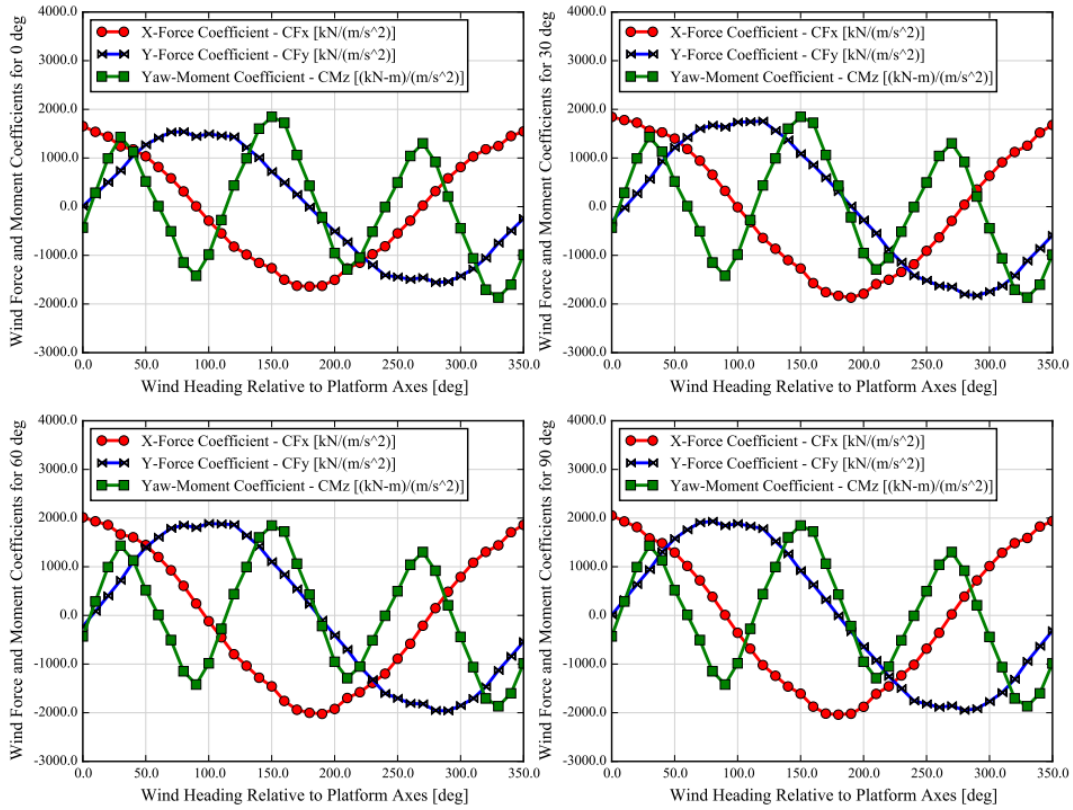


Fig. 4 Wind Force and Moment Load Coefficients of the P-C FWF

3.2 Load cases

Wind headings simulated in coupled analysis are shown in Fig. 5, and characteristics of load cases are reported in Table 5. Six wind speeds, and four headings are considered. The wind speeds considered span the operational range (4 m/s to 25 m/s) of the NREL 5 MW turbine. The Kaimal spectrum is simulated with three groups of turbulence intensity: IEC Class C curve, and fixed values of 10.5% and 8.5% over all wind speeds – these fixed values provide benchmarking to aid understanding of the relationship between Kaimal and Froya responses.

In Table 5, the load case numbers provided are in groups of four, and in each group, the four load cases correspond to the wind headings simulated. For instance, in Load Case Group 1, the Load Case Numbers 1, 2, 3 and 4 correspond to cases simulated with 0 deg, 30 deg, 60 deg and 90 deg respectively. Similarly, in Group 6, Load Case Numbers are 21, 22, 23 and 24 which correspond to 0 deg, 30 deg, 60 deg and 90 deg wind headings respectively. Load cases in Groups 2 to 5 also follow the same pattern of association with wind heading.

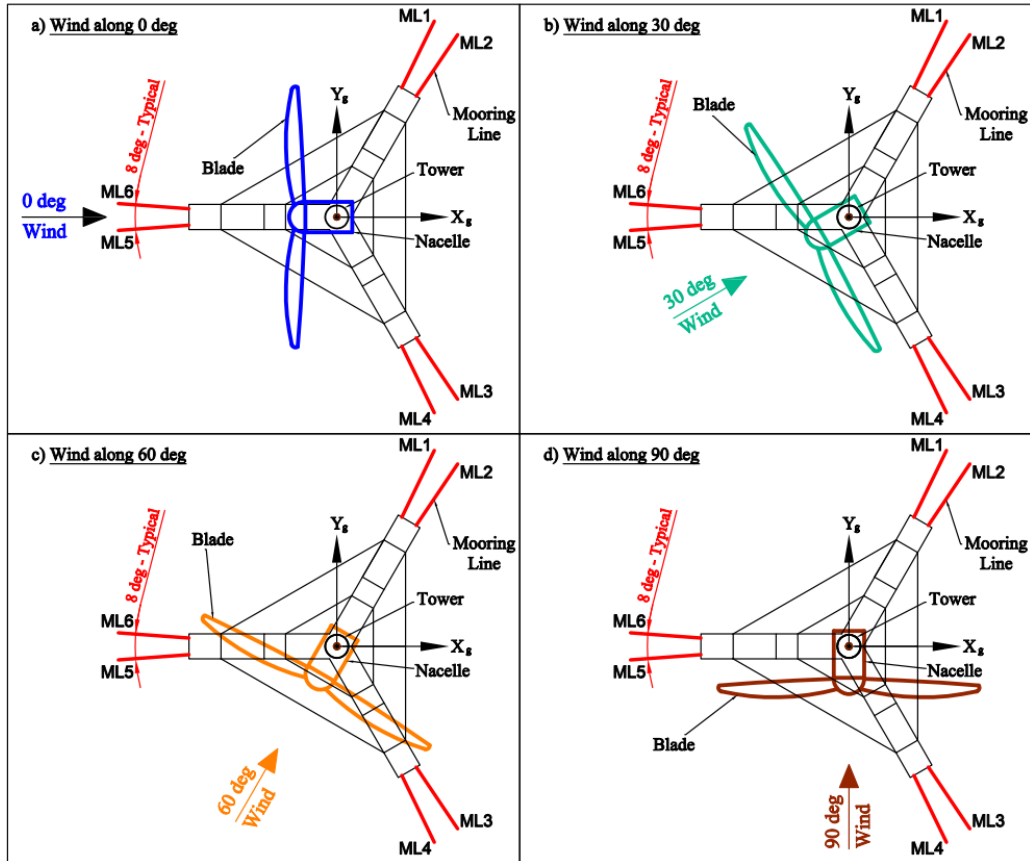


Fig. 5 Wind Headings Simulated in Coupled Analysis

Table 5 Load Case Characteristics

Load Case Group	Hub Height Mean Wind Speed	Platform Mean Wind Speed at 10m above MWL	Load Case Numbers	Wind Spectral Model	Wind Heading
[-]	[m/s]	[m/s]	[-]	[-]	[deg]
1	4.0	2.8	1, 2, 3, 4	Kaimal-IEC Class C Kaimal-10.5% Kaimal-8.5% Froya	0, 30, 60, 90
2	8.0	5.5	5, 6, 7, 8		
3	11.4	7.9	9, 10, 11, 12		
4	16.0	11.0	13, 14, 15, 16		
5	20.0	13.8	17, 18, 19, 20		
6	25.0	17.3	21, 22, 23, 24		

3.3 Representative wind, towerbase and mooring line response spectra

Spectral energy distributions of towerbase shear force, bending moments, and mooring line tensions are discussed in this section to highlight some relevant characteristics. These plots are representative, and are illustrated in Fig. 6, Fig. 7 and Fig. 8. It should be noted in Fig. 6 that two vertical axes are used to show the magnitudes of low and high-frequency responses clearly. The left vertical axis is for low-frequency and the one on the right-hand side is for high-frequency magnitudes. It is observed that low-frequency responses are narrow banded but with higher amplitudes, while high-frequency responses are broad-banded with lower magnitudes. In this study, the low-frequency band is defined as 0 to 0.1 Hz, while the high-frequency band is 0.3 Hz to 0.8 Hz. Since waves are not considered in this study, there is no response in the wave frequency band (0.1 to 0.3 Hz); this is shown in Fig. 6 for towerbase reactions and mooring line tensions. It is noteworthy that even though wind energy extending beyond 0.1 Hz is insignificant as shown in the top left and bottom left subplots for Fig. 7, high-frequency responses still exist – due to coupled interactions of the tower and RNA. This coupling which peaks around 0.52 Hz is discussed in detail in Udoh and Zou (2018).

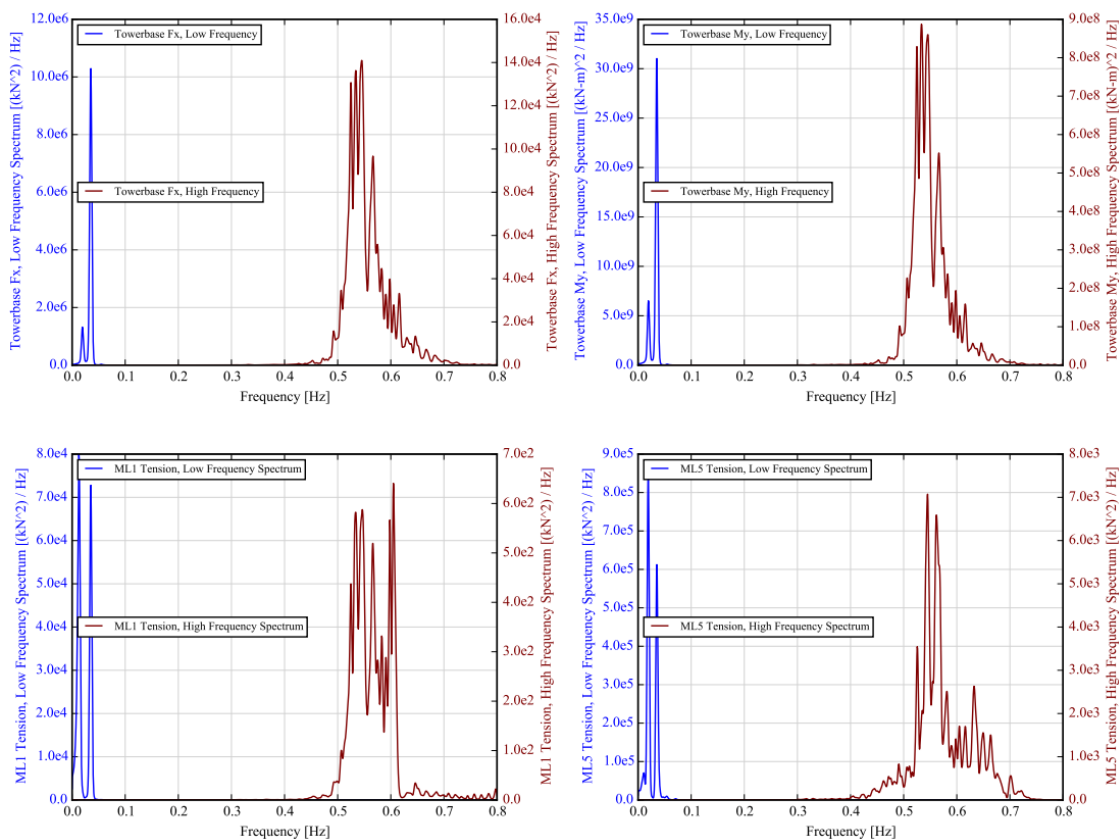


Fig. 6 Representative Energy Spectra of Towerbase Fx, Towerbase My, ML1 and ML5

To illustrate the influence of wind field resolutions on the response spectra, Kaimal and Froya model responses of the towerbase and mooring lines are produced using the wind field resolutions presented in Table 2 and are presented in Figs. 7 and 8. The critical points to note in the spectral distributions are that:

- Wind energy fluctuations vary across the low-frequency region between low-resolution and high-resolution wind grids.
- Consequent upon the variation of wind energy fluctuations for different resolutions, the spectral distributions of towerbase shear force, towerbase bending moment, and mooring line tensions can also vary with wind field resolutions.
- In the low-frequency region (Fig. 7), clear trends of dominance can be seen in the responses between low and high-resolution grids; however, no clear trends exist in the high-frequency region with respect to wind field resolution (Fig. 8).

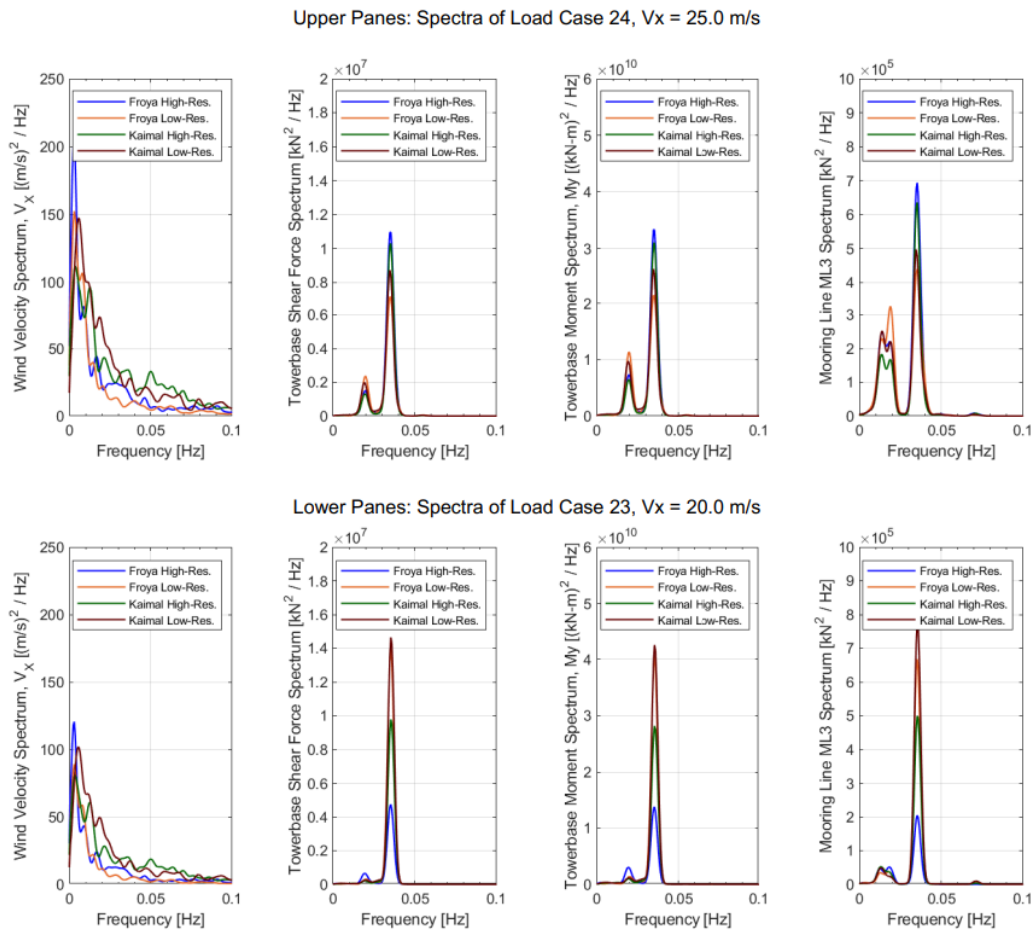


Fig. 7 Energy Spectra of Wind Velocity, Towerbase Fx, Towerbase My, and ML3 for Load Cases 23 (Lower Panes) and 24 (Upper Panes). Only Low-Frequency Region Shown (0 to 0.1 Hz)

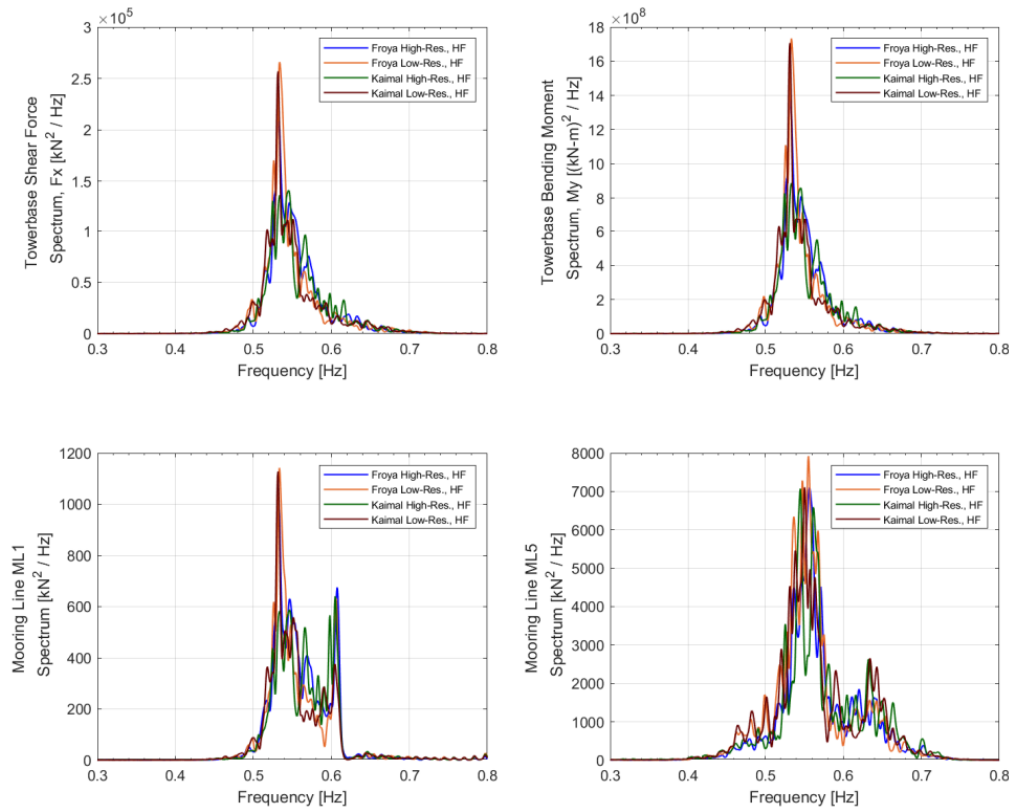


Fig. 8 Energy Spectra of Towerbase Fx, Towerbase My, ML1 and ML5. Upper panes show Force and Moment Spectra; Lower Panes show ML1 and ML5 spectra. Only High-Frequency Region Shown (0.3 to 0.8 Hz)

Fig. 7 shows spectral plots for two load cases (Cases 23 and 24) with mean wind speeds of 20 m/s and 25 m/s – both with the same wind randomization seed number. The spectra indicate that in Case 24, the high-resolution grid has more energy for Kaimal and Froya, and the higher peaks occur at relatively higher frequency than the lower peak. Case 23 presents the reverse, and the dominant peaks have more energy.

4. Results and discussions

4.1 Towerbase Fatigue Potential

Complete fatigue analysis of the towerbase requires structural modeling of the system to accurately determine the stress components and ranges needed to estimate fatigue life. Structural analysis of the system is not covered in this paper, rather the focus is on the wind loading and its potential impact on the structure. DNV-RP-C203 (2011) expresses the fatigue damage accumulation based on S-N fatigue approach, as

$$D = \frac{1}{\bar{a}} \sum_{i=1}^k n_i (\Delta\sigma_i)^m \leq \mu \quad (1)$$

where D is the accumulated fatigue damage, \bar{a} is the intercept of the design S-N curve with the log N axis, n_i is the number of stress cycles in stress block i , $\Delta\sigma_i$ is the stress range in the stress block i , k is the number of stress blocks, m is the inverse slope of the S-N curve, and μ is the usage factor. The stress range in Eq. (1) is known to correlate with response RMS, and number of stress cycles is dependent on the zero-crossing period of the 'load' time history inducing fatigue damage. We can therefore express a representative fatigue potential as:

$$\frac{(RMS)^m}{T_z} \quad (2)$$

where a value of 3.0 is assumed for m , corresponding to S-N curves in seawater for free corrosion (DNV-RP-C203, 2011). The benefit of this formulation is that it amplifies the load RMS values with significant potential to induce fatigue and attenuates negligible values with little significance on fatigue response. Scaling the RMS by the zero-crossing period also enhances the amplification of short-period (or high-frequency) responses which have a major impact on fatigue responses. Long-period loading (with high values of T_z) on the other hand will have relatively less potential on fatigue – for the same RMS value.

Eq. (2) has been used to produce Fig. 9 and Fig. 10 which compare the fatigue potentials for RMS values generated with Kaimal-IEC turbulence intensities (plotted on the horizontal axis), versus the other spectrum types considered (plotted on the vertical axis) in 0, 30, 60 and 90 deg wind conditions. The A-A line in these figures represent the values for which the fatigue potential from Kaimal IEC spectrum is matched by any of the other spectrum types. Therefore, data that fall below the A-A line indicate cases / spectra types which produced less fatigue potential, while data above the line indicate more fatigue potential than the Kaimal-IEC spectrum. Low-frequency (LF) contributions to fatigue potential are denoted with filled shapes, while high-frequency (HF) contributions are represented with hollow shapes. Fig. 8 shows the comparison for towerbase shear force in the global X direction. The general trend seen in the results is that fatigue potential at the towerbases trends with wind speed, and the relative dominance of high-frequency over low-frequency contributions varies with wind heading and/or platform-rotor misalignment. Notable observations in the towerbase shear force include the following;

- The highest fatigue potentials ($\sim 10^6$ kN³/s) are induced under 0, 30 and 60 deg wind conditions, while the lowest values are observed in the 90 deg wind condition. Differences in fatigue potential due to wind heading are primarily driven by the magnitudes of platform wind load coefficients which differ for various platform-rotor misalignments. This observation highlights the towerbase reactions result from a combination of influences induced above the interface (i.e., at the RNA and along the tower), and below the interface at the platform.
- Dominance of high-frequency fatigue potential is seen in 0 deg and 30 deg conditions, with a strong dependence on turbulence intensity. The highest high-frequency fatigue potentials in these two headings are produced by the Kaimal-10.5% spectrum cases with relatively high wind speeds (16 m/s to 25 m/s), and their magnitudes differ only negligibly from the Kaimal-IEC values. Low-frequency contributions to fatigue potential are generally less than high-frequency values for these two headings, but also show a strong dependence on turbulence intensity.
- In 60 deg and 90 deg headings, fatigue potentials trend with wind speed, but the

variation per high or low-frequency is much less, and for some wind speed groups quite insignificant. This indicates that the severity of low or high-frequency contributions to towerbase fatigue, is strongly dependent on rotor-platform misalignment and/or wind heading. High-frequency responses induced by tower-RNA coupling were shown in Udoh and Zou (2018) to be dependent on rotor-platform misalignment – which the authors demonstrated using nacelle accelerations.

- In the 0 and 30 deg conditions wherein the variation of fatigue potential with spectra is significant, the Froya spectrum induces the lowest fatigue potential of all spectrum types and for each wind speed group. In load case group 6 where the wind speed is 25m/s the turbulence intensities of Kaimal-8.5% and Froya are practically equal, the high-frequency fatigue potential of Kaimal-8.5% is at least 20% higher Froya – this indicates that equivalence of turbulence intensity does not necessarily imply equivalent impact on fatigue for different spectrum types. The distribution of energy across different frequencies contributes in driving the differences seen in the fatigue potentials.
- Fatigue potentials of towerbase Fx are lower in the 90 deg condition compared to other headings because the global X axis is a relatively weak response axis when wind loading is at 90 deg.
- Results show that influence of wind spectra on the fatigue potentials diminishes with increasing platform-rotor misalignment. This is observed in 60 deg and 90 deg conditions of towerbase Fx, where the fatigue potentials are either quite close to, or aligned with the A-A line – meaning that the turbulence intensity-dependent dominance on fatigue weakens as the winds shift away from the Xg axis. Variations in fatigue potential with wind spectra are significant in 0 and 30 deg because the magnitudes of aerodynamic-induced loads at the RNA are comparable to the platform wind loads, so that differences in the aerodynamic loads driven by turbulence intensity result in overall variations in the total fatigue potentials. With increasing misalignments (60 and 90 deg) the magnitudes of the platform wind loads become more dominant, such that changes induced by variations in turbulence intensity drive only minimal differences in the overall fatigue potentials.

Observations made in the towerbase Fx are very similar to the trends in towerbase bending moment My (Fig. 10), which is the associated bending moment to Fx.

To further explore the characteristics of low-frequency and high-frequency fatigue potentials with variations in wind heading, towerbase My of each characteristic wind heading are presented in Fig. 11. In this comparison, the horizontal axis is the fatigue potential produced by 0-deg cases, while the vertical axis plots the fatigue potential of all headings including the 0-deg cases. Therefore, data on the A-A line represents fatigue potential of the 0-deg cases. Pertinent observations on the comparisons in Fig. 11 are as follows;

- The highest fatigue potentials are high-frequency components in high wind speed groups regardless of wind spectrum type and wind heading.
- In fatigue potentials around 10^{10} , the highest fatigue potentials are low-frequency components in 60 deg wind heading regardless of wind spectrum type.
- Variations of fatigue potential with wind heading is similar in trend for all Kaimal spectra, but the variations decrease with turbulence intensities. This is consistent with the RMS of towerbase moments trending with turbulence intensity.

- The data scatter characteristics of Kaimal-8.5% and Froya (with turbulence intensity 8.5%) have similar fashion for fatigue potentials in the range 10^8 to 10^{11} $(\text{kN}\cdot\text{m})^3 / \text{s}$ and are different in characteristic when fatigue potential is less than 10^8 $(\text{kN}\cdot\text{m})^3 / \text{s}$.

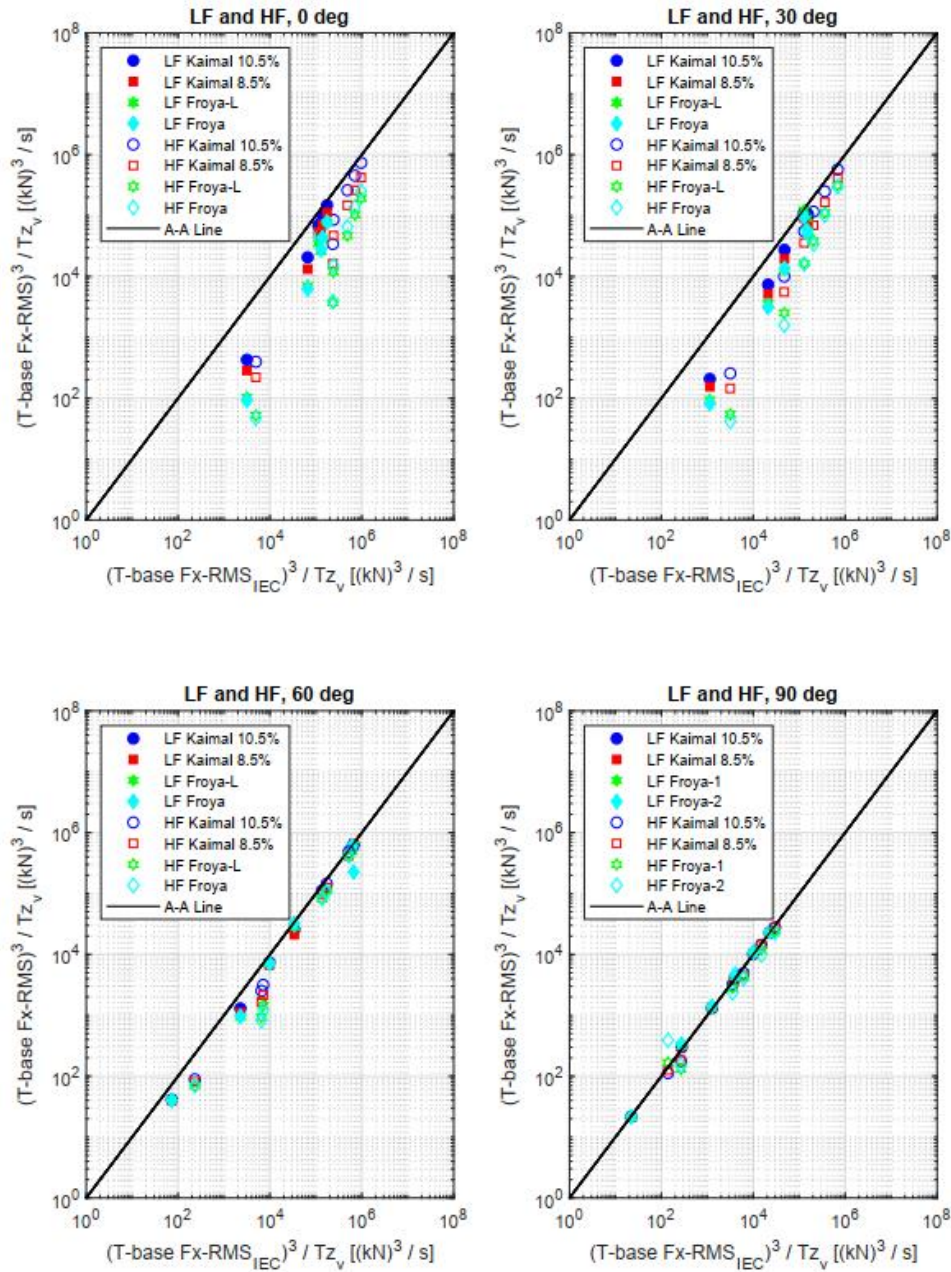


Fig. 9 Towerbase Fx, Low and High-Frequency Fatigue Potentials in 0, 30, 60 and 90 deg Wind

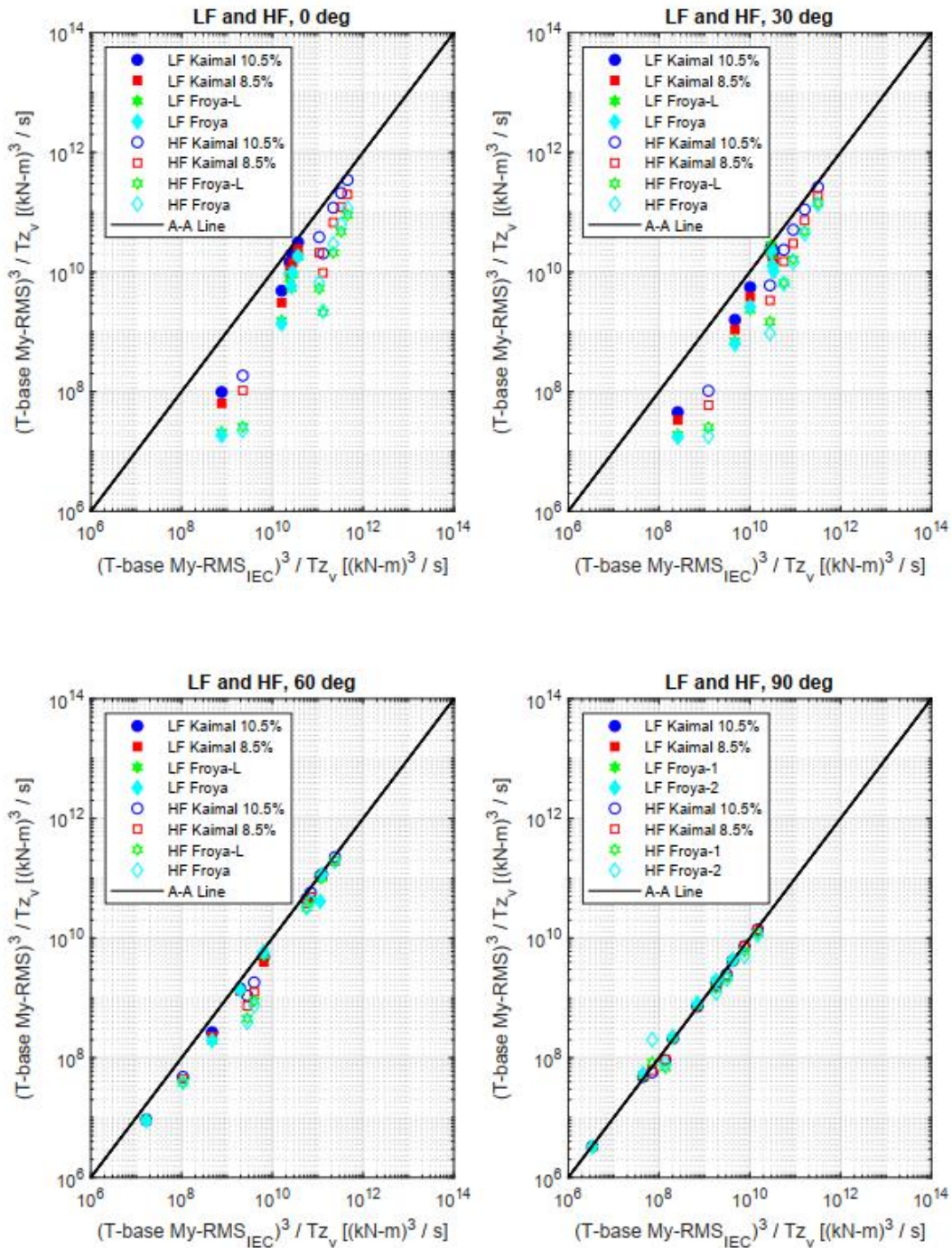


Fig. 10 Towerbase My, Low and High-Frequency Fatigue Potentials in 0, 30, 60 and 90 deg Wind

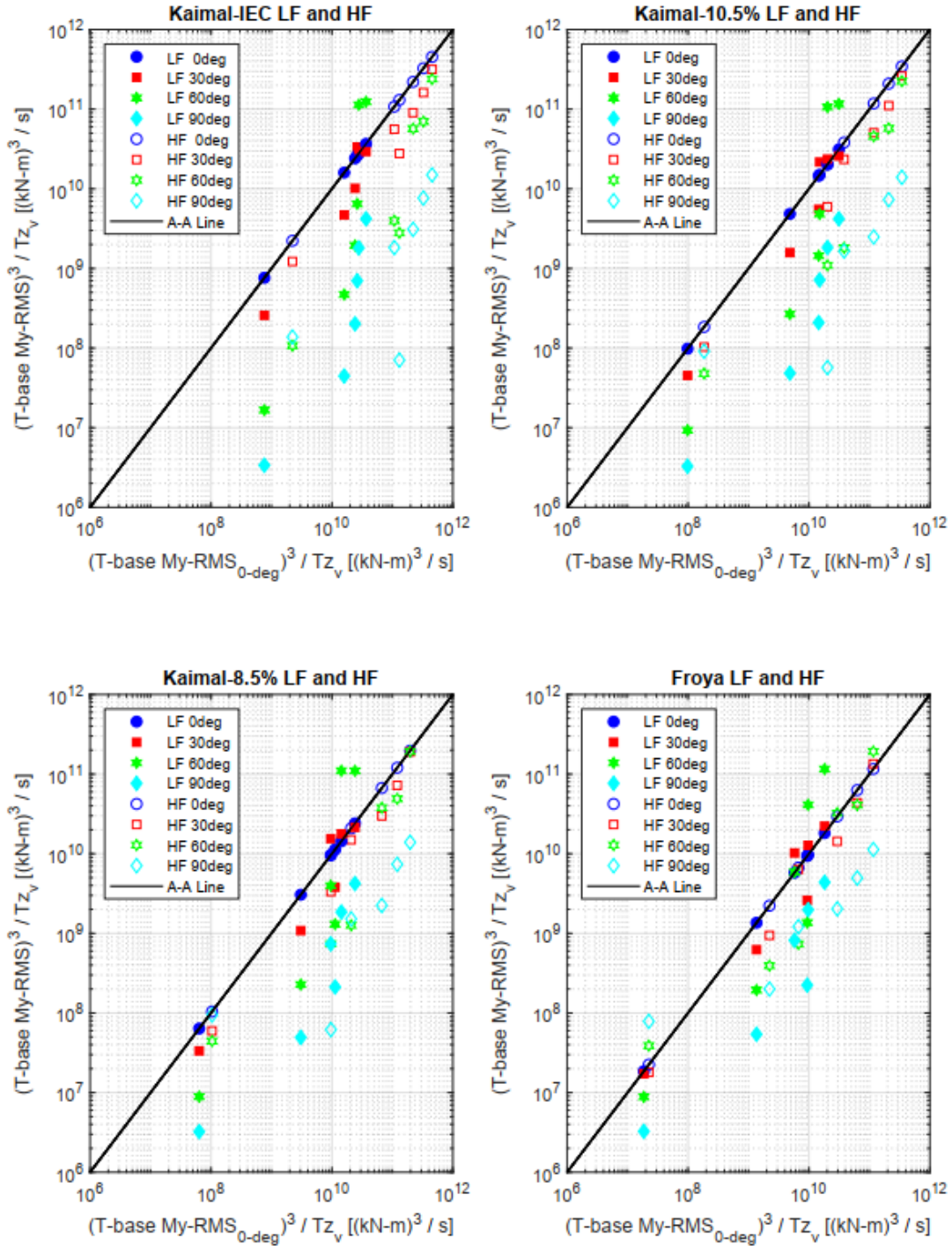


Fig. 11 Towerbase My, Fatigue Potentials Compared by Wind Heading, for Each Spectrum Type

4.2 Mooring line fatigue analysis

Fatigue analysis of mooring lines is performed using the rainflow counting method (Downing and Socie 1982). Although the lines are composed of three components, the fatigue analysis focuses only on the studless chain, which is the top segment and is the most sensitive to fatigue. Parameters implemented in the analysis are presented in Table 6. Assessment of mooring fatigue is done using the fatigue potential introduced earlier, and the actual fatigue damage and life. Like the plots in Section 4.1, the fatigue potentials are compared for mooring lines in Figs. 12-14 respectively. Comparisons in Figs. 12 and 13 are for Mooring Line 1 (ML1) and Mooring Line 5 (ML5) respectively. ML1 and ML5 are selected to represent a downwind (ML1) and an upwind (ML5) line in the system. The fatigue potentials are plotted in the same way as those discussed in Section 4.1 – with Kaimal-IEC values on the horizontal axis and other spectra types plotted on the vertical axis.

Major observations in the mooring line fatigue potentials are summarized as follows;

- In ML1, high-frequency dominance of fatigue potential is only observed in 0 deg wind heading. For all headings, the lowest potentials are low-frequency-induced, but the variation in fatigue potential reduces with increasing platform-rotor misalignment. Trends of fatigue potential are similar for 0 deg and 30 deg between $\sim 10^9$ and $\sim 10^{11}$ kN^3/s , and trends for 60 deg and 90 deg are similar in that at the highest wind speeds little or no variations exist between low-frequency and high-frequency contributions. In 60 and 90 deg wind headings, the low-frequency potentials are closer to the A-A line, especially for the high wind speed cases, whereas the high-frequency potentials are more varied and away from the A-A line. Except for the low wind speeds, fatigue potentials of the other spectrum types are clustered between 10^{10} and 10^{12} kN^3/s in 0 deg and 90 deg. In 60 and 90 deg, there is more linearity between the Kaimal-IEC potentials and other spectrum types.
- Trends in the upwind line ML5 are quite similar to those of ML1, except that;
 - the magnitudes of fatigue potentials are higher due to higher tensions in the upwind lines
 - the variation of high-frequency potentials is stronger across all wind speed groups, especially in the 90 deg heading.

Low-frequency potentials dominate in all headings, and the highest potentials for other spectra types match the Kaimal-IEC potentials.

The observation of low-frequency tensions being the dominant potentials in the mooring lines is not at all surprising, since the platform motions which are predominantly low-frequency motions dampen the high-frequency responses to coming from the tower and RNA, to some extent. Conversely, it is interesting although the wind loads are predominantly low-frequency loads, high-frequency mooring line tensions induced by coupled interactions between the tower and RNA are not negligible compared to the low-frequency values.

Table 6 T-N Curve Parameters for Mooring Line Fatigue Analysis

m	K	Reference Breaking Strength
[-]	[-]	[kN]
3.0	563.74	8844

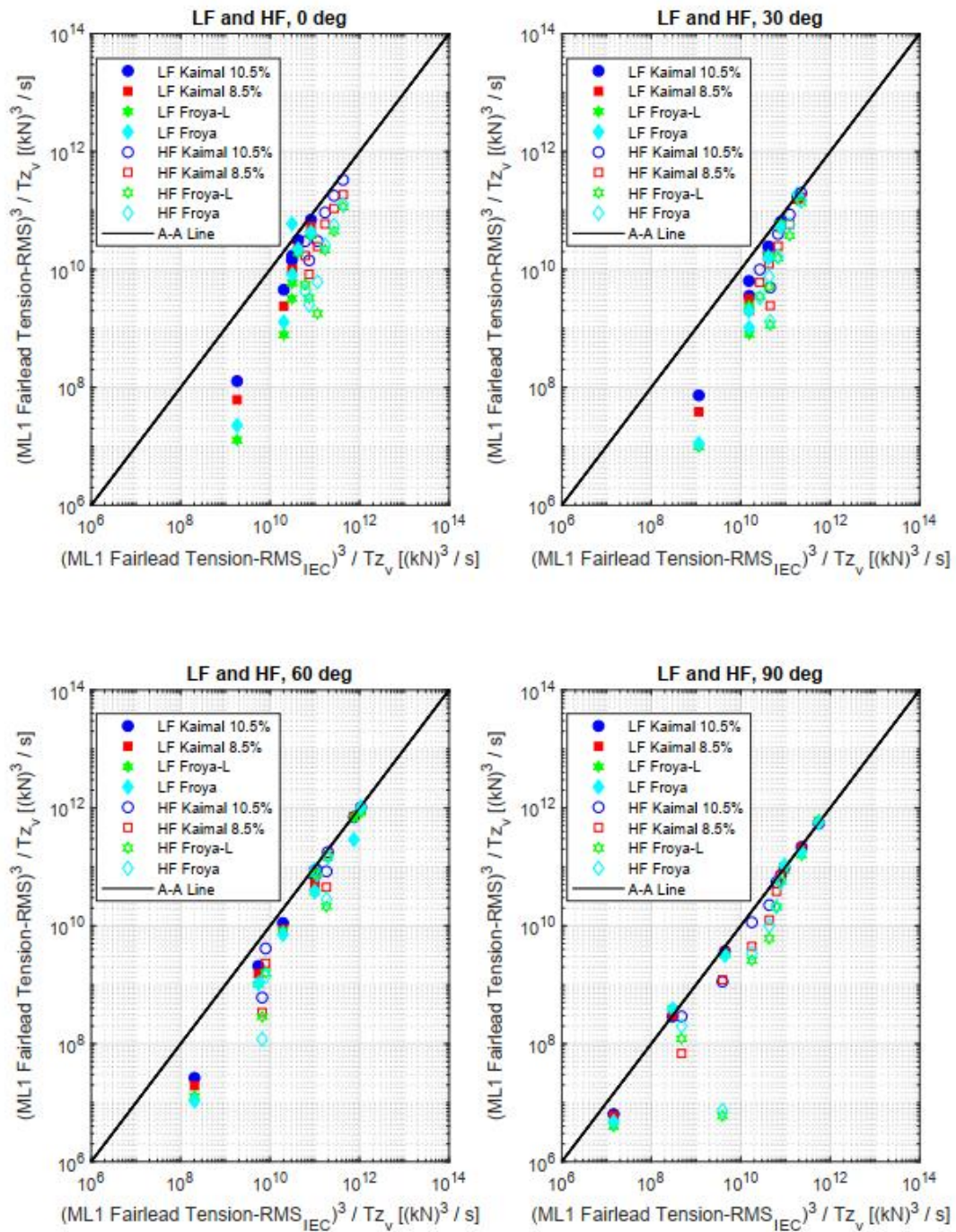


Fig. 12 ML 1 Low and High-Frequency Fatigue Potentials in 0, 30, 60 and 90 deg Wind

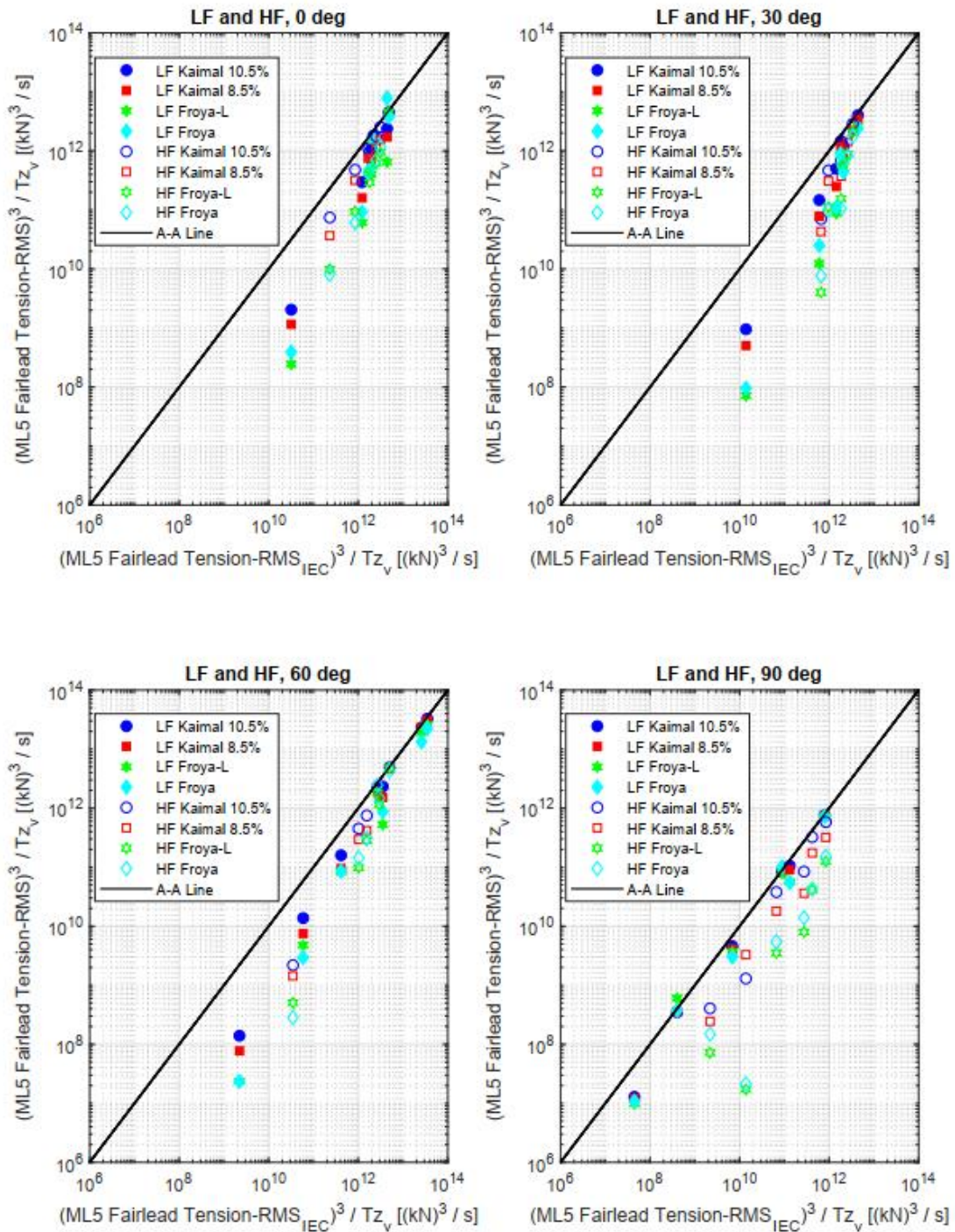


Fig. 13 ML 5 Low and High-Frequency Fatigue Potentials in 0, 30, 60 and 90 deg Wind

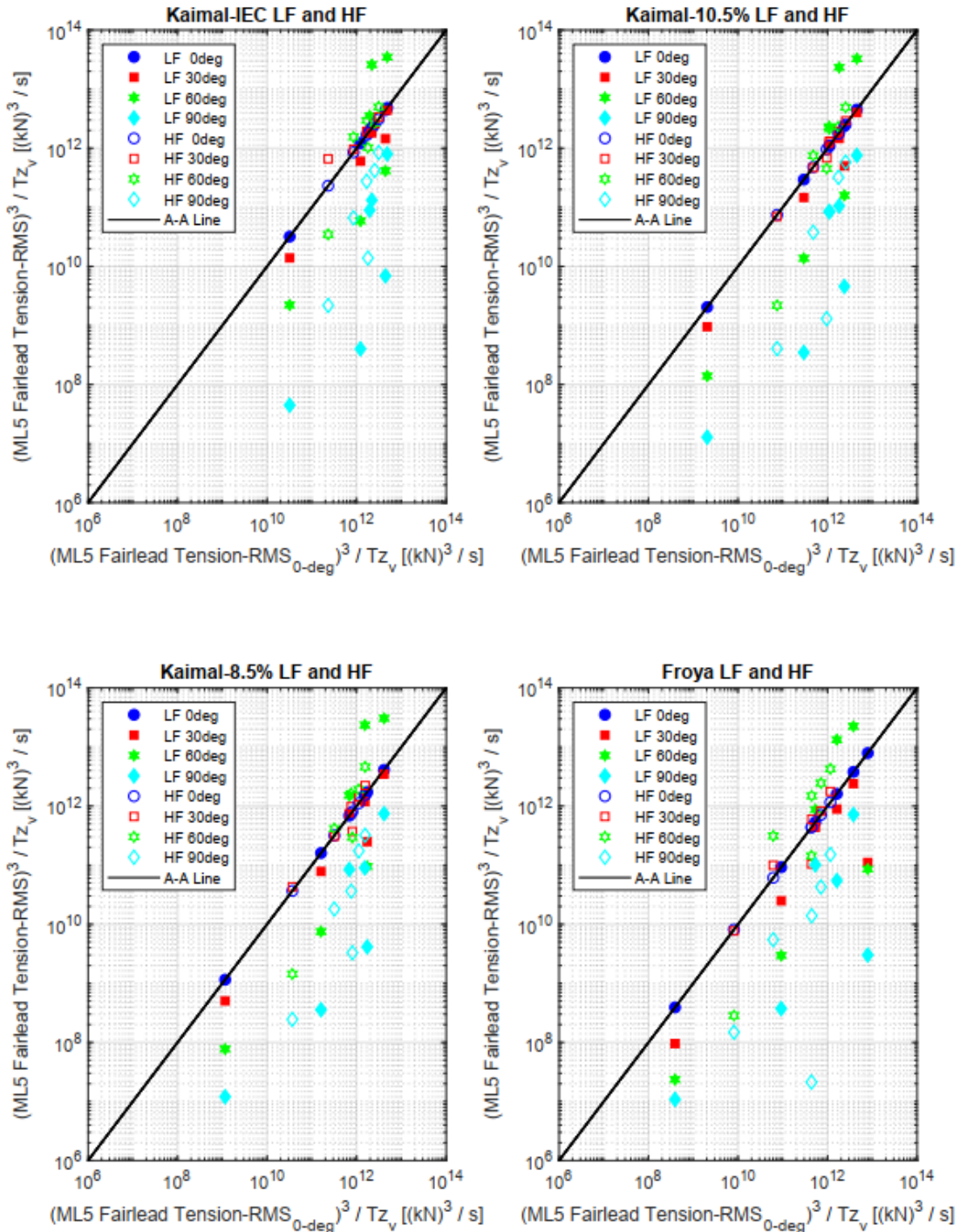


Fig. 14 ML5 Fatigue Potentials Compared by Wind Heading, for Each Spectrum Type

To examine the influence of wind heading or rotor misalignment on the fatigue potentials, comparisons are presented in Fig. 14 for each spectrum type – this comparison is only made for ML5. Results show the following notable observations:

- The highest fatigue potentials are low-frequency potentials produced by the 60 deg cases with high wind speed, followed by high-frequency potentials in the same heading; this is consistent with resultant wind load coefficients of the platform in 60 deg heading which exceed those of other headings.
- At low wind speeds, fatigue potential decreases with increasing platform-rotor misalignment; this trend is consistent across all spectrum types.

A clear delineation of low-frequency and high-frequency contributions to the fatigue potential is presented in Fig. 15 for the four spectrum types and all six mooring lines. Overall, there is more low-frequency contribution than high-frequency across all spectrum types but some notable high-frequency contributions exist – like the ~50% contribution seen in ML2 of Kaimal-IEC, and ~40% contributions in ML3 of Kaimal-IEC, ML2 of Kaimal-10.5%, ML3 of Kaimal-8.5% and ML3 of Froya. The lowest ratio of high-frequency to low-frequency contributions is observed in the Froya model. Fig. 16 shows the comparison of mooring line fatigue damage per year across the different wind speed groups to provide insights as to the relative contributions to damage. Fatigue damage reported assume equal probability of wind speeds, and as such the variations are driven by damage induced by each wind speed, per mooring line. If unequal probabilities were applied in analysis, the trends of accumulated fatigue damage would change depending on product of fatigue probabilities and damage. The plots indicate the highest damage is caused by group 6 which has the highest wind speed of 25 m/s, and the lines most affected are the upwind lines which experience the highest tensions when loaded from the 0 – 90 deg sector. Fatigue damage is also shown to reduce with turbulence intensity from Kaimal-IEC to Froya. To ensure that these results are interpreted in the correct context, it is necessary to emphasize that the relative magnitudes of low-frequency and high-frequency mooring line tensions (and all other results discussed in this paper) exclude wave effects (i.e., wind-only scenario); the presence of wave dynamics may influence the relative magnitudes. However, the purpose of this study is to understand the wind spectra-induced effects, and as such the results are insightful to the extent required.

Fig. 17 is a 3-dimensional representation of the total fatigue damage per year for all mooring lines, with the third dimension being the spectrum type. Total damage in Kaimal-IEC cases exceed all else, while the upwind lines experience the most damage. The main points highlighted here are that the turbulence intensity is a dominant factor in the fatigue damage of mooring lines, and that upwind lines are more susceptible to fatigue damage (caused mostly by low-frequency potential, based on Fig. 15) than intermediate lines (ML3 and ML4) or downwind lines (ML1 and ML2).

Ratios of fatigue damage per year between Froya and Kaimal models are summarized in Table 7 and displayed in Fig. 18 to quantitatively put the previous comparisons into context. The ratios are calculated using annual accumulated fatigue damage of the Froya model as the benchmark or denominator, such that the ratios for the Froya model are 1.0 for all lines. The two wind speed groups with the most dominant accumulated damage – Groups 5 and 6, are used for these comparisons. As given in Table 7 and illustrated in Fig. 18, fatigue damage of the Kaimal models exceed those of Froya by factors ranging from 1.1 to 2.6. The most significant dominance is observed in Group 5 of Kaimal-IEC, for ML4. These factors directly indicate the excessive conservatism which could be inadvertently built into the fatigue design, if the Kaimal model (with relatively high turbulence intensities) is implemented where the suitable wind model should have been an offshore site-based model, such as Froya. Even for Kaimal-8.5% which has practically the

same turbulence intensity as Froya at 25 m/s, the exceedance factors are between 40% and 60% in the upwind mooring lines (ML5 and ML6) which are more susceptible to fatigue damage. This finding reveals the importance of correctly choosing wind spectrum type as well as associated turbulent intensity in fatigue analysis.

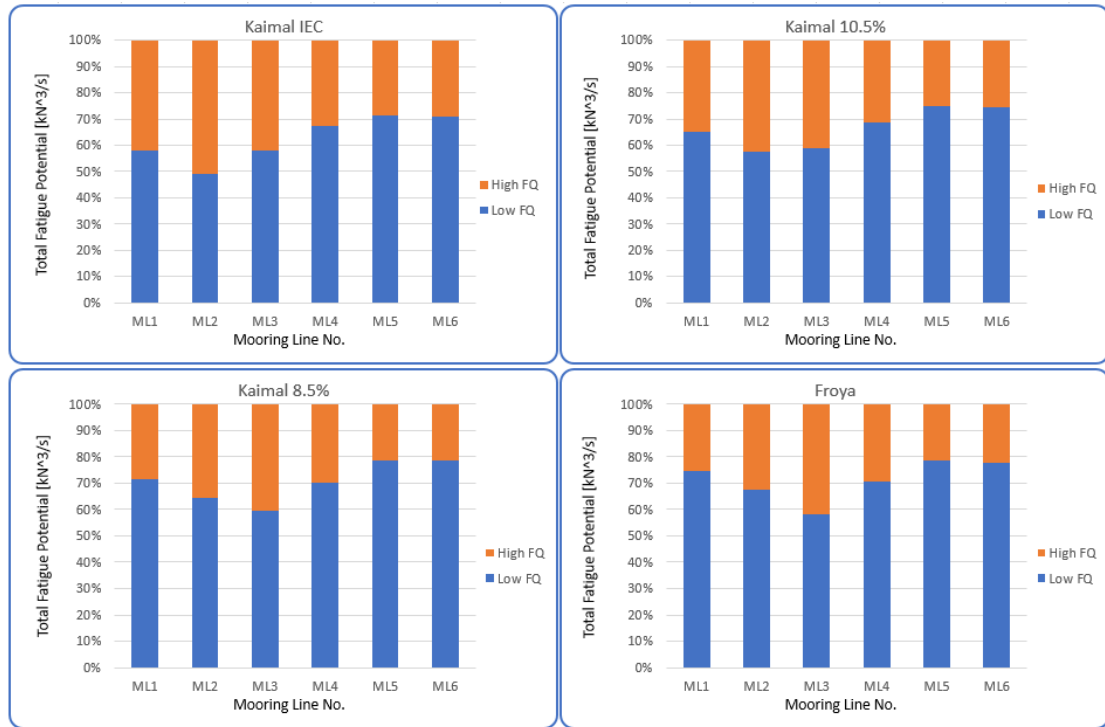


Fig. 15 Mooring Line Fatigue Potential, Low and High-Frequency Comparison

Table 7 Ratios of Accumulated Fatigue Damage per Year – Groups 5 and 6

Mooring Line	Froya		Kaimal-8.5%		Kaimal-10.5%		Kaimal-IEC	
	Group 5	Group 6	Group 5	Group 6	Group 5	Group 6	Group 5	Group 6
ML1	1.0	1.0	1.6	1.0	1.8	1.2	2.2	1.3
ML2	1.0	1.0	1.5	1.0	1.7	1.2	2.1	1.4
ML3	1.0	1.0	1.8	1.1	2.0	1.2	2.4	1.3
ML4	1.0	1.0	2.0	1.1	2.2	1.2	2.6	1.3
ML5	1.0	1.0	1.5	1.4	1.6	1.5	1.9	1.6
ML6	1.0	1.0	1.6	1.4	1.7	1.5	2.0	1.7

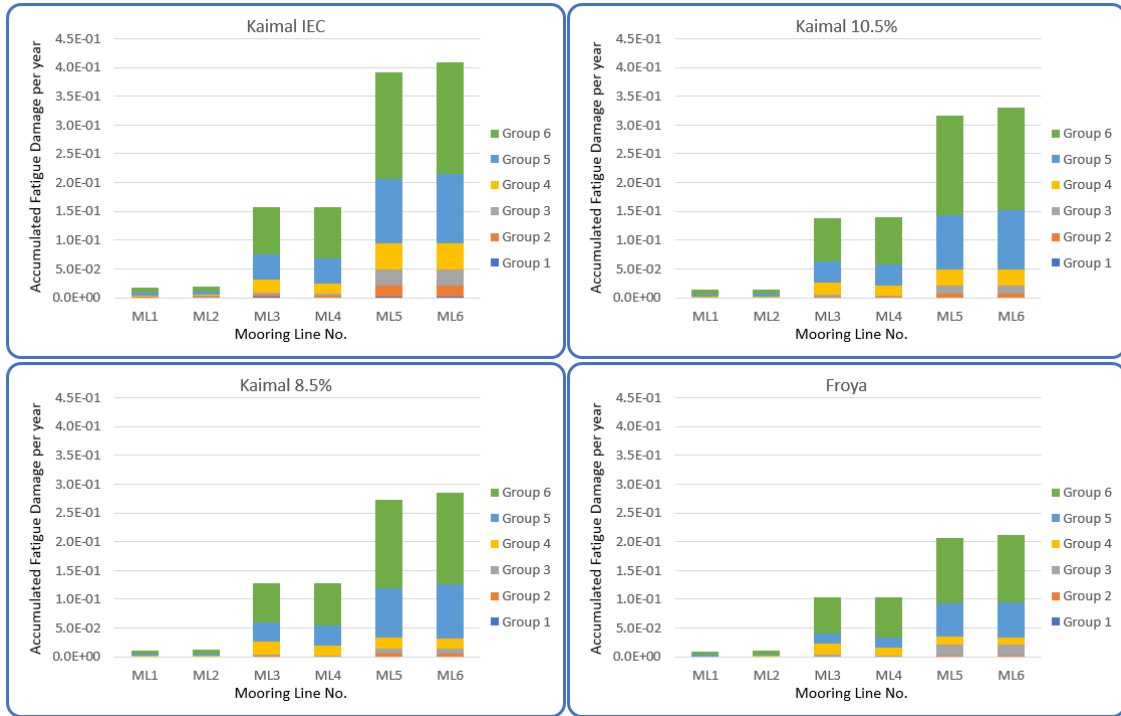


Fig. 16 Annual Mooring Line Fatigue Damage in Load Case Groups

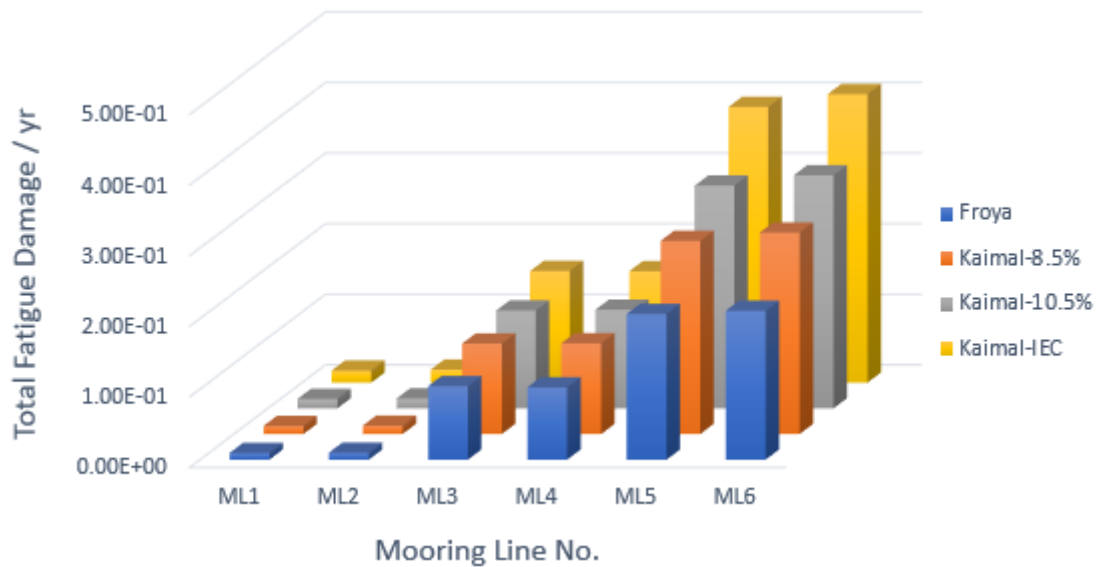


Fig. 17 Total Mooring Line Fatigue Damage Per Year, for All Spectra Types

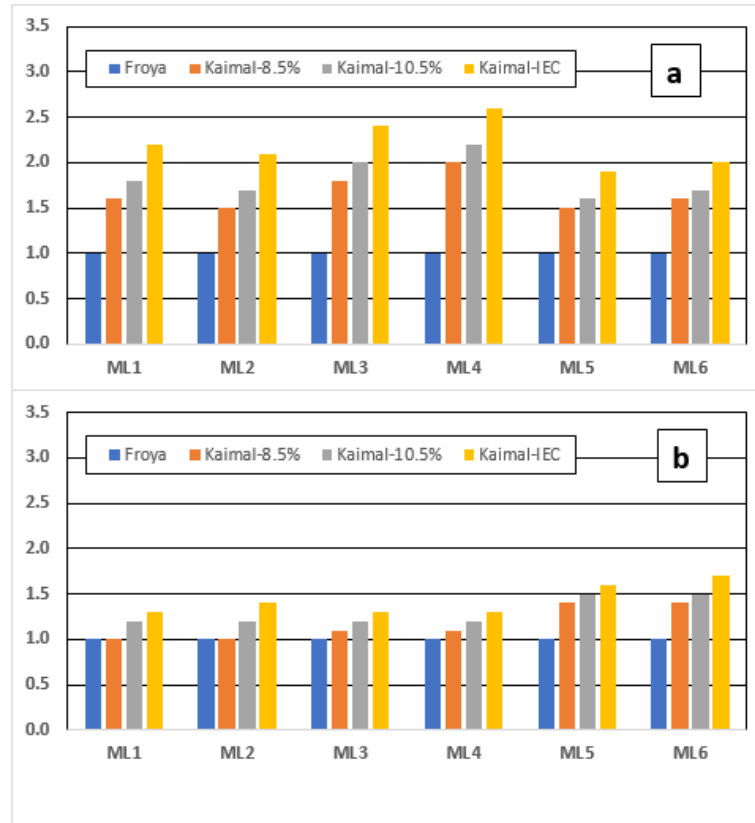


Fig. 18 Ratios of Accumulated Fatigue Damage per Year: (a) Group 5 and (b) Group 6

The impact of wind grid resolution on mooring line fatigue was assessed by simulating all 24 load cases once with the low-resolution wind grid, and once with the high-resolution wind grid – and the simulated mooring line tensions post-processed in fatigue analysis. Wind field resolutions reported in Table 2 were used in the simulations, and the results are plotted in Fig. 19. Results show that the low-resolution wind grid gives more conservative estimates of fatigue life for almost all the cases. It indicates that the distribution of low-frequency versus high-frequency energy in the responses is skewed towards high-frequency with more significant margins when the low-resolution wind grid is implemented in analysis. While it can be argued that this may be an artifact of numerical modeling, it is a real issue that can drive major changes in fatigue design of mooring lines. Fatigue life for ML1 and ML2 are high, considering that the damage which these lines experienced were the lowest. ML5 and ML6 have the lowest fatigue lives since they have the highest accumulated damage.

Some interesting observations in Fig. 19 are highlighted as follows:

- Among Kaimal spectra, the differences between high- and low- resolution wind grids become more pronounced as the turbulence intensities decrease. In other words, high-resolution wind grid is more important for lower turbulence intensity wind field modeling.

Between Kaimal spectrum and Froya spectrum with same turbulence intensity (8.5%), high-resolution wind grid is more crucial for Kaimal type wind spectrum.

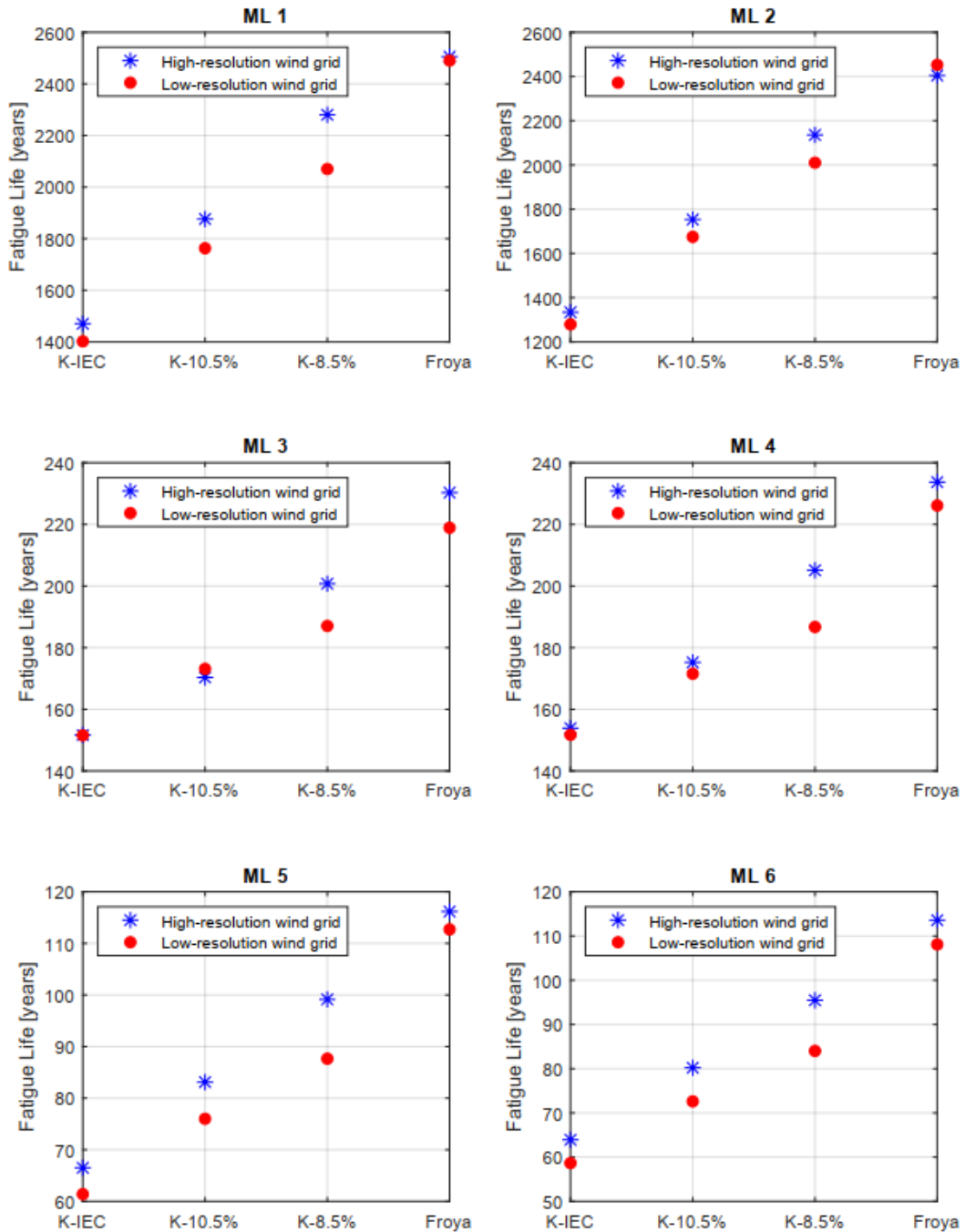


Fig. 19 Mooring Line Fatigue Life per Spectra Type and Wind Field Resolution

5. Conclusions

Fatigue responses of the towerbase and mooring lines of an FOWT have been systematically assessed with respect to the spectral characteristics of turbulent winds. Conclusions made here are within the context of the assumption that the Froya spectral model may be extrapolated / applied to mean wind speeds below 10 m/s to assess the fatigue behavior of FOWTs. Results presented indicate that considerable penalties can be encountered in fatigue design if incorrect parameters are implemented in analysis – leading to significantly higher costs that could be avoided in offshore wind projects. The main conclusions drawn are highlighted as follows:

- 1) Characteristics of wind spectrum used in analysis – most importantly turbulence intensity, should adequately represent actual site conditions to minimize unwarranted conservatism in design. The challenges associated with obtaining site-specific data for projects are real; however, in the absence of such data engineering judgement must be applied in developing a representative data set and wind spectra for analysis and design to keep the resulting design costs realistic.
- 2) The sensitivity of fatigue design to wind field modeling has been clearly demonstrated in this paper. Variations in fatigue life between low-resolution and high-resolution wind field grids are quite significant (up to 12% in some cases – Fig. 18). This finding supports the need for due diligence in analysis; sensitivity studies for wind grids to be applied in coupled analysis is necessary for obtaining realistic responses.
- 3) In an aerodynamic-hydrodynamic-elastic coupled system, there are significant high-frequency contributions to the mooring fatigue, as displayed in Fig. 15 even with wind only. Ignoring coupling effects and high-frequency contributions will result in considerable underestimations of fatigue damage.
- 4) This paper emphasizes the void which currently exists in the offshore wind industry, regarding adequate guidelines for offshore wind modeling. Guideline organizations such as the IEC should strongly consider providing more accurate and clearer recommendations for turbulence intensities and wind modeling for offshore sites. This will lessen the chances of erroneous assumption or implementation of land-based models and data (which are clearly more conservative than necessary) in offshore wind projects.

Acknowledgments

This study was funded by Atkins, a member of the SNC-Lavalin group. We appreciate Atkins' continuous support of research and development in offshore wind.

References

- Anderson, O.J. and Løvseth, J. (1992), "The maritime turbulent wind field. measurements and models", Final Report for Task 4 of the Statoil Joint Industry Project, Norwegian Institute of Science and Technology, Trondheim, Norway.
- Anderson, O.J. and Løvseth, J. (2006), "The Frøya database and maritime boundary layer wind

- description”, *Mar. Struct.*, **19**, 173-192.
- Bir, G. (2005), “User’s guide to BMODES (Software for computing rotating beam coupled modes)”, Technical Report, National Renewable Energy Laboratory, NREL/TP-500-39133, Golden CO. USA.
- Det Norske Veritas (2011), Recommended Practice DNV-RP-C203, *Fatigue Design of Offshore Steel Structures*, 12-2.
- Downing, S.D. and Socie, D.F. (1982), “Simple rainflow counting algorithms”, *Int. J. Fatigue*, **4**(1), 31-40.
- Homb, R.H. (2013), “Fatigue analysis of mooring lines on floating wind turbine hywind demo”, Master’s Thesis, Norwegian University of Science and Technology.
- International Electrotechnical Commission (2005), IEC 61400-1, *International Standard on Wind Turbines, Part 1: Design Requirements*, Third Edition, 1301-1328.
- International Electrotechnical Commission (2009), IEC 61400-3 (BS EN 61400-3), *International Standard on Wind Turbines, Part 3: Design Requirements for Offshore Wind Turbines*.
- Jonkman, B.J. and Buhl, M.L., Jr. (2005), “FAST user’s guide”, Technical Report, National Renewable Energy Laboratory, NREL/TP-500-38230, Golden CO. USA.
- Jonkman, B.J. and Kilcher, L. (2012), “Turbsim user’s guide”, Technical Report, National Renewable Energy Laboratory, Golden CO. USA.
- Jonkman, J. Butterfield S., Musial, W. and Scott, G. (2009), “Definition of a 5-MW reference wind turbine for offshore system development”, Technical Report, National Renewable Energy Laboratory, NREL/TP-500-38060, Golden CO. USA.
- Kaimal, J.C., Wyngaard, J.C., Haugen, D.A., Cote, O.R. and Izumi, Y. (1976), “Turbulence structure in the convective boundary layer”, *J. Atmosph. Sci.*, **33**(417), 2152-2169.
- Kaimal, J.C., Wyngaard, J.C., Izumi, Y. and Cote, O.R. (1972), “Spectral Characteristics of Surface-layer Turbulence”, *J. Roy.Meteorol. Soc.*, **98**(417), 563-589.
- Maritime Research Institute Netherlands (2007), “Wind Loads on Offshore Structures (WINDOS), User Guide for WINDOS Engineering Tool”.
- Masciola, M., Robertson A., Jonkman, J. and Driscoll, F. (2011), “Investigation of a FAST-OrcaFlex Coupling Module for Integrating Turbine and Mooring Dynamics of Offshore Floating Structures”, National Renewable Energy Laboratory, NREL/CP-5000-52896, Golden CO. USA.
- Masciola, M., Robertson, A., Jonkman, J., Coulling, A. and Goupee, A., “Assessment of the Importance of Mooring Dynamics on the Global Response of the DeepCwind Floating Semisubmersible Offshore Wind Turbine”, International Offshore and Polar Engineering Conference, June 30 – July 5, Anchorage, Alaska, USA.
- Orcina Ltd., OrcaFlex User Manual, version 9.7, www.orcina.com.
- Udoh, I.E. and Zou, J. (2016), “Wind turbulence effects in global responses of a 5 MW wind turbine TLP”, *Proceedings of the 21ST Offshore Symposium – Texas Section of the Society of Naval Architects and Marine Engineers*, Houston, USA, February.
- Udoh, I.E. and Zou, J. (2018), “Wind spectral characteristics on strength design of floating offshore wind turbines”, *Ocean Syst. Eng.*, **8**(3), 281-312.
- Udoh, I.E., Zou, J. and Edgar, C. (2016), “Impacts of wind turbulence on the performances of s semi-submersible type and TLP-type wind turbine”, *Proceedings of the Offshore Technology Conference*, OTC-27261-MS, Houston, USA, May.
- WAMIT Inc. (2006), WAMIT User Manual, version 6.4, Massachusetts Institute of Technology and www.wamit.com.

Appendix

Distributed Mass and Flexural Properties of the Tower

Segment Number	Tower Height from Base	Mass Density	Fore-Aft Stiffness	Side-to-Side Stiffness	Torsional Stiffness	Axial Stiffness	Fore-Aft Mass inertia	Side-to-Side Mass inertia	Fore-Aft Mass offset	Side-to-Side Mass offset
	[m]	[kg/m]	[Nm ²]	[Nm ²]	[Nm ²]	[N]	[kg-m]	[kg-m]	[m]	[m]
1	0.000	17340.4	1.064E+12	1.064E+12	9.96E+11	2.532E+11	52395.2	52395.2	0.0	0.0
2	0.035	12483.8	9.371E+11	9.371E+11	8.78E+11	2.290E+11	46160.7	46160.7	0.0	0.0
3	0.069	12355.7	8.984E+11	8.984E+11	8.41E+11	2.258E+11	44235.4	44235.4	0.0	0.0
4	0.104	9835.3	6.305E+11	6.305E+11	5.90E+11	1.623E+11	31043.5	31043.5	0.0	0.0
5	0.138	9742.6	6.036E+11	6.036E+11	5.65E+11	1.599E+11	29722.3	29722.3	0.0	0.0
6	0.173	6112.6	5.065E+11	5.065E+11	4.74E+11	1.380E+11	24940.3	24940.3	0.0	0.0
7	0.207	6031.1	4.842E+11	4.842E+11	4.53E+11	1.359E+11	23842.7	23842.7	0.0	0.0
8	0.242	5212.2	4.021E+11	4.021E+11	3.77E+11	1.153E+11	19802.6	19802.6	0.0	0.0
9	0.276	5141.9	3.839E+11	3.839E+11	3.59E+11	1.135E+11	18904.0	18904.0	0.0	0.0
10	0.311	5054.3	3.619E+11	3.619E+11	3.39E+11	1.113E+11	17823.0	17823.0	0.0	0.0
11	0.345	7502.4	3.452E+11	3.452E+11	3.23E+11	1.096E+11	16999.5	16999.5	0.0	0.0
12	0.380	4933.0	3.329E+11	3.329E+11	3.12E+11	1.083E+11	16394.3	16394.3	0.0	0.0
13	0.414	4863.1	3.170E+11	3.170E+11	2.97E+11	1.065E+11	15607.1	15607.1	0.0	0.0
14	0.449	4776.0	2.977E+11	2.977E+11	2.79E+11	1.043E+11	14661.2	14661.2	0.0	0.0
15	0.483	4723.8	2.866E+11	2.866E+11	2.68E+11	1.030E+11	14113.2	14113.2	0.0	0.0
16	0.518	4653.8	2.722E+11	2.722E+11	2.55E+11	1.012E+11	13401.5	13401.5	0.0	0.0
17	0.552	4566.7	2.548E+11	2.548E+11	2.39E+11	9.904E+10	12547.8	12547.8	0.0	0.0
18	0.587	4497.1	2.415E+11	2.415E+11	2.26E+11	9.729E+10	11893.8	11893.8	0.0	0.0
19	0.621	4427.3	2.287E+11	2.287E+11	2.14E+11	9.553E+10	11259.4	11259.4	0.0	0.0
20	0.656	4357.3	2.163E+11	2.163E+11	2.02E+11	9.376E+10	10647.9	10647.9	0.0	0.0
21	0.690	5694.3	2.043E+11	2.043E+11	1.91E+11	9.200E+10	10059.0	10059.0	0.0	0.0
22	0.725	4217.6	1.928E+11	1.928E+11	1.81E+11	9.024E+10	9492.3	9492.3	0.0	0.0
23	0.759	4147.7	1.817E+11	1.817E+11	1.70E+11	8.848E+10	8947.2	8947.2	0.0	0.0
24	0.794	4078.2	1.711E+11	1.711E+11	1.60E+11	8.673E+10	8426.3	8426.3	0.0	0.0
25	0.828	4008.7	1.609E+11	1.609E+11	1.51E+11	8.498E+10	7926.0	7926.0	0.0	0.0
26	0.863	3938.8	1.512E+11	1.512E+11	1.42E+11	8.322E+10	7443.3	7443.3	0.0	0.0
27	0.897	3868.9	1.418E+11	1.418E+11	1.33E+11	8.145E+10	6980.6	6980.6	0.0	0.0
28	0.932	3799.0	1.328E+11	1.328E+11	1.24E+11	7.969E+10	6537.4	6537.4	0.0	0.0
29	0.966	3736.2	1.250E+11	1.250E+11	1.17E+11	7.811E+10	6155.5	6155.5	0.0	0.0
30	1.000	4565.2	1.184E+11	1.184E+11	1.11E+11	7.670E+10	5829.2	5829.2	0.0	0.0